4-14-2020

Human iPSC-derived neurons and cerebral organoids establish differential effects of germline NF1 gene mutations

Corina Anastasaki

Michelle L Wegscheid

Kelly Hartigan

Jason B Papke

Nathan D Kopp

See next page for additional authors

Authors

Corina Anastasaki, Michelle L Wegscheid, Kelly Hartigan, Jason B Papke, Nathan D Kopp, Jiayang Chen, Olivia Cobb, Joseph D Dougherty, and David H Gutmann

Stem Cell Reports
Report
ISSCR
OPEN ACCESS

Human iPSC-Derived Neurons and Cerebral Organoids Establish Differential Effects of Germline *NF1* Gene Mutations

Corina Anastasaki,[1,4] Michelle L. Wegscheid,[1,4] Kelly Hartigan,[1] Jason B. Papke,[1] Nathan D. Kopp,[2,3] Jiayang Chen,[2] Olivia Cobb,[1] Joseph D. Dougherty,[2] and David H. Gutmann[1,*]
[1]Department of Neurology, Washington University School of Medicine, Box 8111, 660 S. Euclid Avenue, St. Louis, MO 63110, USA
[2]Department of Genetics, Washington University School of Medicine, St. Louis, MO, USA
[3]David Geffen School of Medicine at UCLA, Los Angeles, CA, USA
[4]Co-first author
*Correspondence: gutmannd@wustl.edu
https://doi.org/10.1016/j.stemcr.2020.03.007

SUMMARY

Neurofibromatosis type 1 (NF1) is a common neurodevelopmental disorder caused by a spectrum of distinct germline *NF1* gene mutations, traditionally viewed as equivalent loss-of-function alleles. To specifically address the issue of mutational equivalency in a disease with considerable clinical heterogeneity, we engineered seven isogenic human induced pluripotent stem cell lines, each with a different NF1 patient *NF1* mutation, to identify potential differential effects of *NF1* mutations on human central nervous system cells and tissues. Although all mutations increased proliferation and RAS activity in 2D neural progenitor cells (NPCs) and astrocytes, we observed striking differences between *NF1* mutations on 2D NPC dopamine levels, and 3D NPC proliferation, apoptosis, and neuronal differentiation in developing cerebral organoids. Together, these findings demonstrate differential effects of *NF1* gene mutations at the cellular and tissue levels, suggesting that the germline *NF1* gene mutation is one factor that underlies clinical variability.

INTRODUCTION

Neurofibromatosis 1 (NF1; OMIM 162200) is a neurogenetic condition characterized by remarkable phenotypic variability, where affected children develop a wide variety of central nervous system (CNS) pathologies, ranging from brain tumors and motor delays to learning difficulties, attention deficits, and autism (Fisher et al., 2018; Hyman et al., 2006; Jett and Friedman, 2010; Korf, 2013; Morris and Gutmann, 2018). One of many potential factors underlying this clinical variability could be the specific *NF1* germline mutation, a notion suggested by population-based studies (Anastasaki et al., 2017; Bolcekova et al., 2013; Kehrer-Sawatzki et al., 2017; Koczkowska et al., 2018; Pinna et al., 2015; Rojnueangnit et al., 2015; Sharif et al., 2011; Trevisson et al., 2019; Upadhyaya et al., 2007). For example, patients harboring the c.2970–2971_delAAT, c.5425C > T, and c.3112A > G *NF1* germline mutations lack dermal and plexiform neurofibromas, the signature peripheral nervous system tumors in NF1 (Pinna et al., 2015; Trevisson et al., 2019; Upadhyaya et al., 2007).

Although these studies raise the possibility that not all *NF1* gene mutations are functionally equivalent, they do not establish differential effects of *NF1* patient germline mutations at the cellular or tissue levels, a critical step in interpreting the significance of reported genotype-phenotype associations. To specifically evaluate differential *NF1* mutation effects on human CNS cells and tissues, while controlling for important confounding factors (e.g., sex, genomic differences), we generated an isogenic series of human induced pluripotent stem cells (hiPSCs) harboring seven representative NF1-patient *NF1* mutations.

RESULTS AND DISCUSSION

Generation of Isogenic *NF1*-Mutant hiPSCs

The seven *NF1* pathogenic mutations, derived from patients in our clinic population at Washington University/St. Louis Children's Hospital, represent the spectrum of mutations typically seen in individuals with NF1. In this regard, the selected mutations were interspersed throughout the *NF1* protein (neurofibromin) coding sequence, were both proximal and distal to the well-characterized RAS GTPase-activating protein (RAS-GAP) domain (GRD), and included four nonsense (c.1149C > A, c.2041C > T, c.6513T > A, c.6619C > T), one splice site (c.1185+1G > A), one missense (c.5425C > T), and one frameshift (c.3431-32_dupGT) mutation (Figures 1A, S1, and S2). All of the engineered isogenic hiPSCs harbored only a single *NF1* mutation ("*NF1*-mutant"), retained expression of the remaining wild-type *NF1* allele as confirmed by DNA and RNA sequencing (Figure S1), and expressed similar levels of *NF1* mRNA (Figure 1B). For all hiPSC lines with two clones, identical results were obtained using numerous independently generated biological replicates, as well as with three NF1 patient-derived hiPSC lines generated from somatic cells (fibroblasts; Figure S3, Table S1).

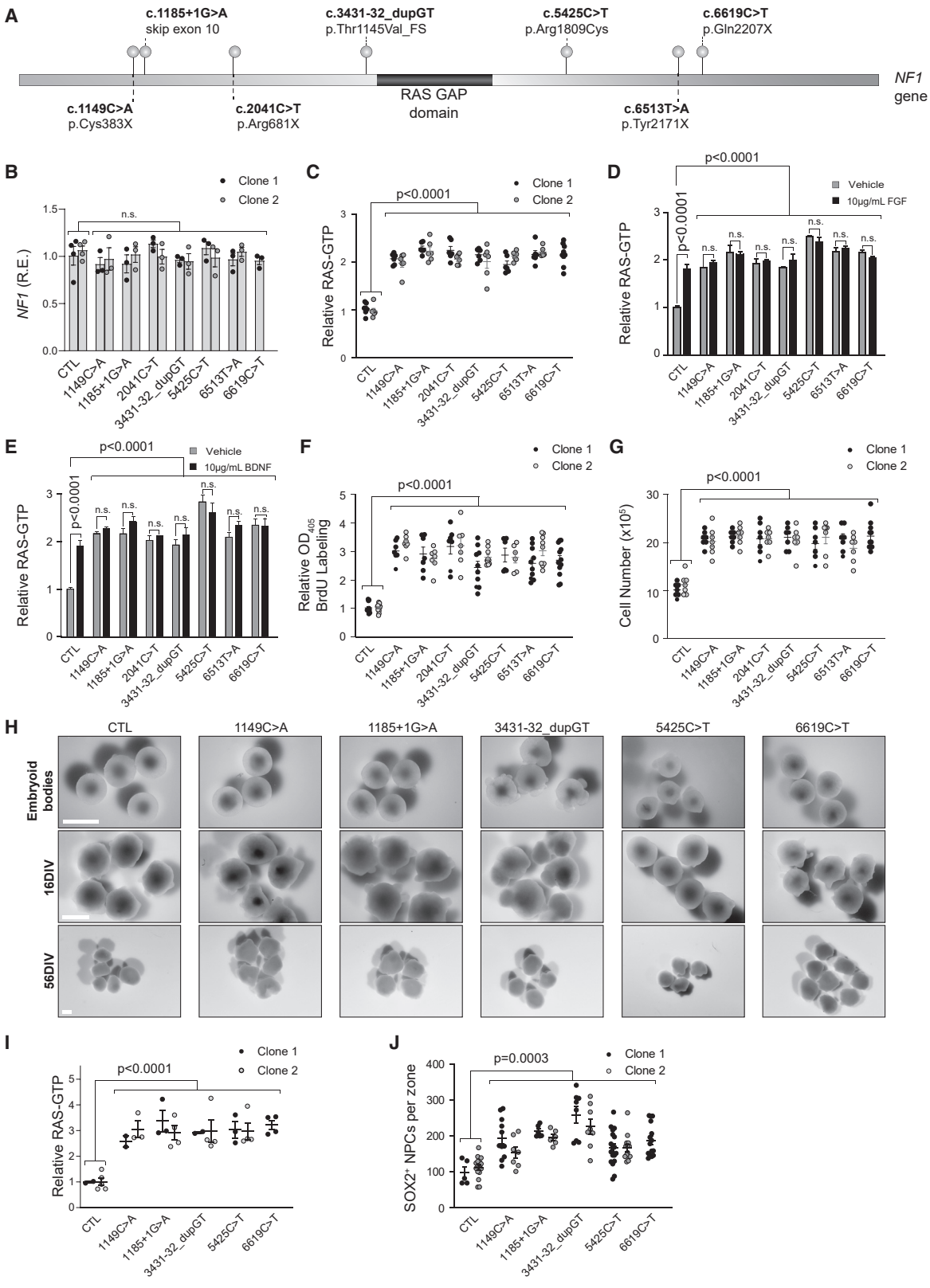

(legend on next page)

Isogenic *NF1*-Mutant hiPSC-Derived NPCs and Astroglia Have Increased RAS Activity and Proliferation

To determine the consequence of the different *NF1* gene mutations on neurofibromin signal transduction and function in human CNS cells, *NF1*-mutant and control hiPSCs were first differentiated into neural progenitor cells (NPCs) capable of generating both neurons (TUJ1$^+$ cells) and glia (S100β$^+$ cells) (Figure S2B). Because neurofibromin primarily functions as an RAS-GAP to control cell proliferation, we initially assessed RAS activity. Consistent with this negative RAS regulatory property, all *NF1*-mutant NPCs exhibited a comparable 1.8- to 2.2-fold increase in RAS-GTP relative to the isogenic control (Figure 1C). Importantly, the addition of growth factors (fibroblast growth factor [FGF] or brain-derived neurotrophic factor [BDNF]) did not further increase RAS activity in the *NF1*-mutant lines, but resulted in greater RAS-GTP levels in the control lines, equivalent to the levels observed in the unstimulated *NF1*-mutant lines (Figures 1D and 1E). These findings demonstrate that a heterozygous *NF1* mutation phenocopies the effect of exogenous growth factor stimulation on RAS activation. In addition, all *NF1*-mutant NPCs exhibited increased cell division, as demonstrated by increased bromodeoxyuridine (BrdU) incorporation (2.6- to 3.2-fold increase; Figure 1F) and total cell number (1.9- to 2-fold increase; Figure 1G). To evaluate the effects of distinct *NF1* gene mutations on the production of NPCs in a 3D model of human brain development, we generated cerebral organoids from the control and *NF1*-mutant hiPSC lines. Despite repeated efforts, we were unable to derive organoids from two of the seven *NF1*-mutant hiPSC lines (c.2041C > T and c.6513T > A), but successfully generated organoids from the control and five of the seven *NF1*-mutant hiPSC lines (c.1149C > A, c.1185+1G > A, c.3431-32_dupGT, c.5425C > T, c.6619C > T; Figure 1H). The organoids formed radially organized ventricle-like structures populated by SOX2$^+$ NPCs by 16 days *in vitro* (DIV). Similar to the 2D cultures, all *NF1*-mutant organoids exhibited a 2.8- to 3.2-fold increase in RAS activity (Figure 1I), as well as a 1.6- to 2.2-fold increase in total NPCs per ventricular zone at 16 DIV (Figure 1J).

Next, we sought to determine whether these heterozygous *NF1* mutational effects were observed in another proliferating CNS cell type by differentiating the NPCs into astrocytes (Figure 2A). Similar to the NPCs, *NF1*-mutant astrocytes exhibited 2- to 2.3-fold increased RAS activity (Figure 2B), 2.3- to 2.7-fold increased cell division (Figure 2C), and 2.1- to 2.5-fold greater total cell number (Figure 2D) relative to the control line. Consistent with the 2D astrocytes, 56 DIV *NF1*-mutant organoids had more EAAT1- and GFAP-expressing cells (astrocytes) (Figure 2E) compared with control organoids. Importantly, isogenic *NF1*-mutant NPCs and organoids were similar to those of their respective patient-derived NPCs (c.1185+1G > A; c.5425C > T; c.6513T > A) and organoids (c.1185+1G > A; c.5425C > T) (Figures S3 and S4; Table S1) in RAS activity and NPC proliferation, as well as to whole-brain lysates from genetically engineered mice harboring the analogous germline *Nf1* gene mutations (c.1149C > A, c.2041C > T, c.3431-32_dupGT, and c.5425C > T; Figure 3A). Taken together, these data illustrate that all heterozygous *NF1* mutations increase RAS activity and RAS-regulated cell proliferation in both human and murine CNS cells.

hiPSC-Derived *NF1*-Mutant Neurons Exhibit Both Shared and Differential Deficits in 2D Cultures

As some children with NF1 exhibit cognitive deficits and neurodevelopmental delays (Hyman et al., 2005, 2006; Jett and Friedman, 2010; Morris and Gutmann, 2018), we sought to determine the effects of distinct *NF1* germline mutations on human CNS neuronal function and differentiation. Based on the observation that *Nf1*-mutant (*Nf1*+/−) mice exhibit increased GABAergic tone that contributes to the observed deficits in learning and spatial memory (Costa et al., 2002; Cui et al., 2008), we assayed

Figure 1. Isogenic *NF1*-Mutant hiPSC-Derived NPCs Exhibit Increased RAS Activity and Cell Proliferation

(A) Schematic diagram illustrating the position of the engineered NF1 patient mutations within the *NF1* gene. The location of the RAS-GAP domain is highlighted in black.

(B) Relative *NF1* mRNA expression in isogenic *NF1*-mutant NPCs is similar to the controls.

(C–E) (C) Quantitation demonstrating increased RAS activity (RAS-GTP) in isogenic *NF1*-mutant NPCs relative to controls (CTL) before and after the addition of (D) 10 μg/mL FGF or (E) BDNF. A minimum of three independent replicates was performed for each treatment condition.

(F) BrdU incorporation is increased by 2.6- to 3.2-fold in *NF1*-mutant NPCs relative to control NPCs.

(G) 1.9- to 2-fold increases in total cell numbers were observed in *NF1*-mutant NPCs compared with controls.

(H) Representative bright-field images of embryoid bodies and cerebral organoids at 16 and 56 DIV.

(I and J) (I) Quantitation demonstrating increased RAS activity (2.8- to 3.2-fold) and (J) increased numbers of SOX2$^+$ NPCs per ventricular zone (1.6- to 2.2-fold) in 16 DIV *NF1*-mutant cerebral organoids relative to control organoids.

Each dot represents an independently generated data point derived from separate experiments and the two different clones for each line are denoted as black versus gray dots. All data are represented as means ± SEM. (B, C, F, G, I, and J) One-way ANOVA with Tukey post-test. (D and E) Two-way ANOVA with Bonferroni post-test. n.s., not significant. Scale bar, 1 mm.

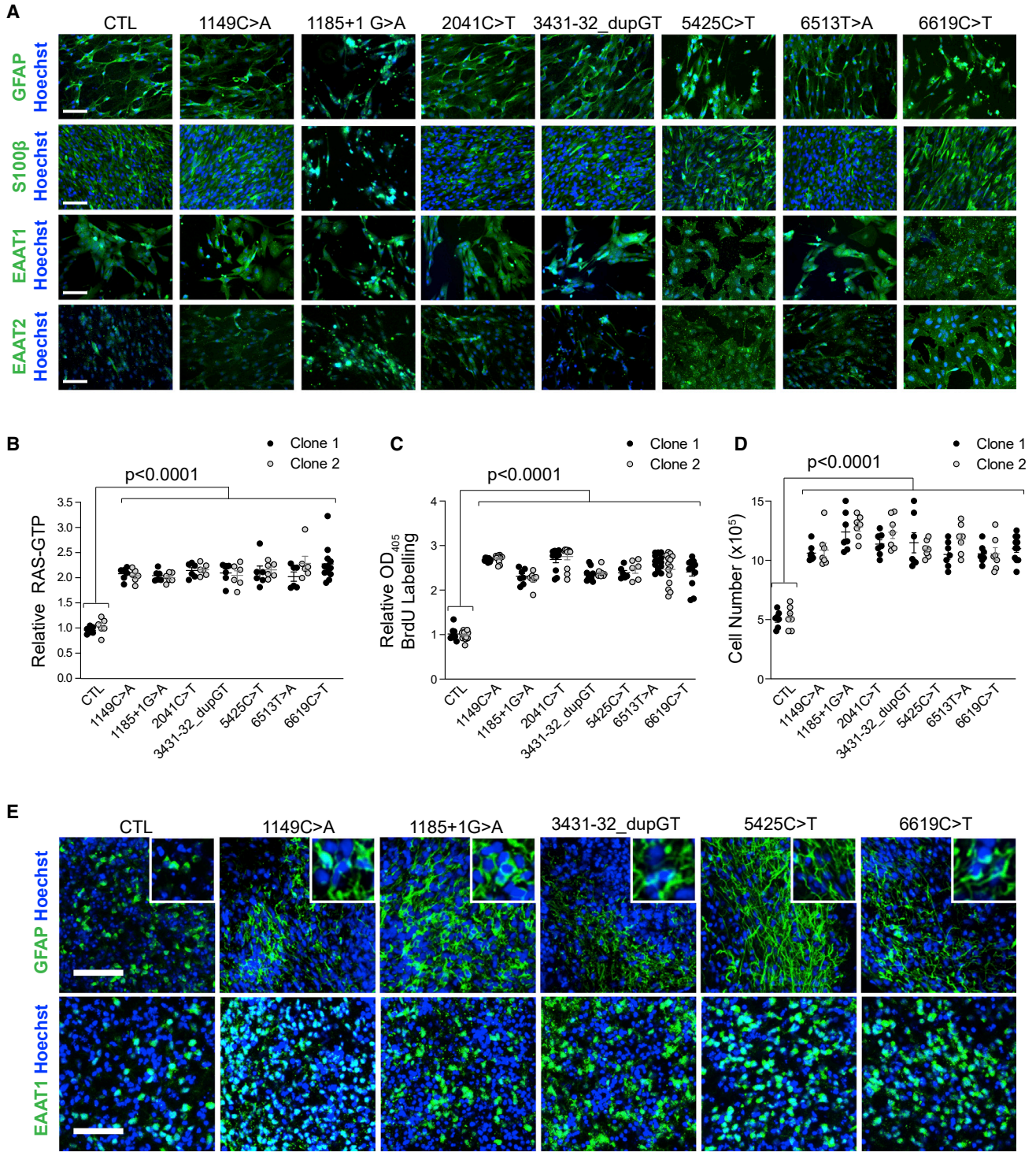

Figure 2. hiPSC-Derived *NF1*-Mutant Astroglia Exhibit Increased RAS Activity and Cell Proliferation

(A) *NF1*-mutant and control NPCs were differentiated into GFAP$^+$, S100$^+$, EAAT1$^+$, and EAAT2$^+$ astrocytes in 2D cultures. Scale bar, 100 μm.

(B) RAS-GTP was increased by 2- to 2.3-fold in *NF1*-mutant astrocytes relative to controls (CTL).

(C) Proliferation of *NF1*-mutant astrocytes was 2.3- to 2.7-fold higher relative to controls.

(D) Direct cell counting demonstrated a 2.1- to 2.5-fold increase in *NF1*-mutant astrocytes compared with controls.

(legend continued on next page)

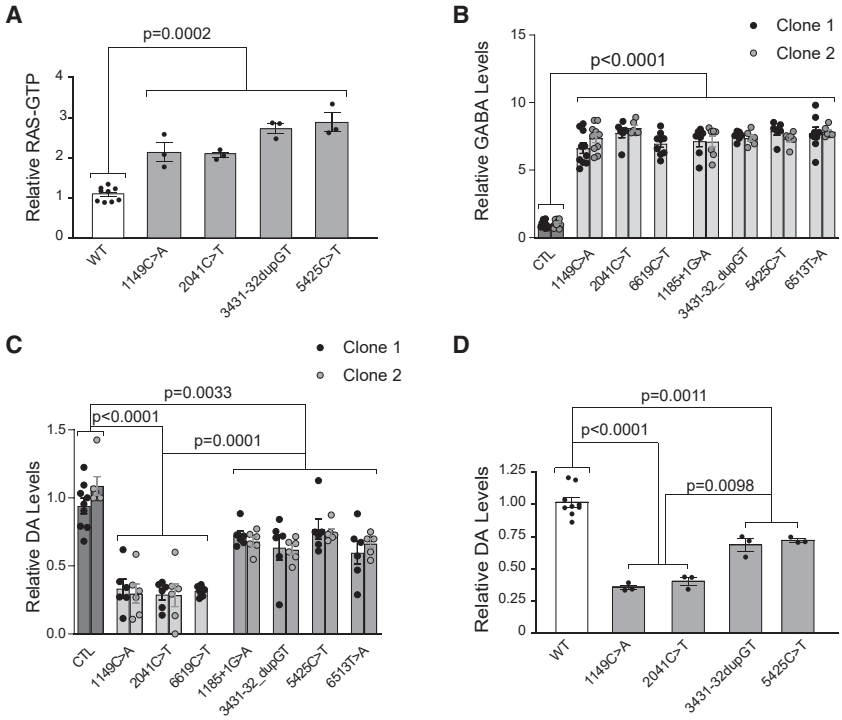

Figure 3. hiPSC-Derived *NF1*-Mutant Neurons, NPCs, and *Nf1*-Mutant Mice Display Molecular Similarities and Differences

(A) *Nf1*-mutant (1149C > A, 2041C > T, 3431-32_dupGT, 5425C > T) genetically engineered mouse brain lysates exhibit increased RAS activity compared with wild-type littermate controls.

(B) GABA levels are increased in all *NF1*-mutant NPC-derived neurons relative to controls.

(C and D) Dopamine levels are differentially reduced in (C) *NF1*-mutant NPCs relative to controls and (D) *Nf1*-mutant genetically engineered mouse brain lysates compared with WT littermate controls.

Each dot represents an independently generated data point derived from separate experiments and the two different clones for each line are denoted as black versus gray dots. All data are represented as means ± SEM. One-way ANOVA with Tukey post-test.

GABA levels in NPC-derived GABAergic neurons (Figures 3B and S3E). In all *NF1*-mutant neurons (2D cultures), GABA levels were increased (6.5- to 7.8-fold) relative to isogenic control neurons, revealing a shared abnormality in all *NF1*-mutant GABAergic neurons.

In contrast, *NF1*-mutant NPCs in 2D cultures displayed striking differences in dopamine (DA) (Figure 3C) levels. DA levels were reduced by >70% in the c.1149C > A, c.2041C > T, and c.6619C > T *NF1* mutants, but by <40% in the c.1185+1G > A, c.3431-32_dupGT, c.5425C > T, and c.6513T > A *NF1* mutants relative to the control line. These differential effects mirror findings using patient-derived NPCs (Figures S3E and S3F; Table S1) (Anastasaki et al., 2015), as well as mice engineered with NF1 patient-specific *Nf1* germline mutations (Figure 3D) (Toonen et al., 2016). Taken together, these findings demonstrate the existence of differential effects of *NF1* germline mutations on neuronal differentiation *in vitro*.

Differential Effects of *NF1* Mutations on Cerebral Organoid NPC Proliferation, Apoptosis and Differentiation

To further explore the differential effects of *NF1* mutations in the developing human brain, we used the more contextually relevant cerebral organoid platform. Examination of NPC proliferation, apoptosis and neuronal differentiation in 16 DIV cerebral organoids revealed two distinct groups of *NF1* mutants (Figure 4): group 1 (c.1185+1G > A; c.5425C > T; c.6619C > T) *NF1* mutants exhibited increased NPC proliferation (1.3- to 1.4-fold) and apoptosis (2- to 3-fold), but had similar numbers of early (NeuroD1$^+$, TUJ1$^+$) and late (MAP2$^+$) immature neurons relative to controls. In this manner, group 1 *NF1* mutations increased both proliferation and apoptosis during NPC differentiation, allowing neurogenesis to proceed normally. In contrast, group 2 (c.1149C > A; c.3431-32_dupGT) *NF1*-mutant organoids had normal NPC proliferation, but reduced NPC apoptosis (70%–92% reduction) and very few immature neurons relative to the isogenic controls (73%–84% reduction). In this latter group, the reduction in NPC death was coupled with a delay in neurogenesis, suggesting that inappropriate survival of NPC subpopulations creates a barrier to initiating timely neuronal differentiation. Importantly, these observations persist in patient-derived cerebral organoids harboring the same mutations (Figure S4; Table S1).

(E) *NF1*-mutant cerebral organoids grown for 56 DIV had increased cells with GFAP$^+$ fibers and increased numbers of EAAT1$^+$ glial cells compared with isogenic controls. Scale bars, 50 μm.

Each dot represents an independently generated data point derived from separate experiments and the two different clones for each line are denoted as black versus gray dots. All data are represented as means ± SEM. One-way ANOVA with Tukey post-test.

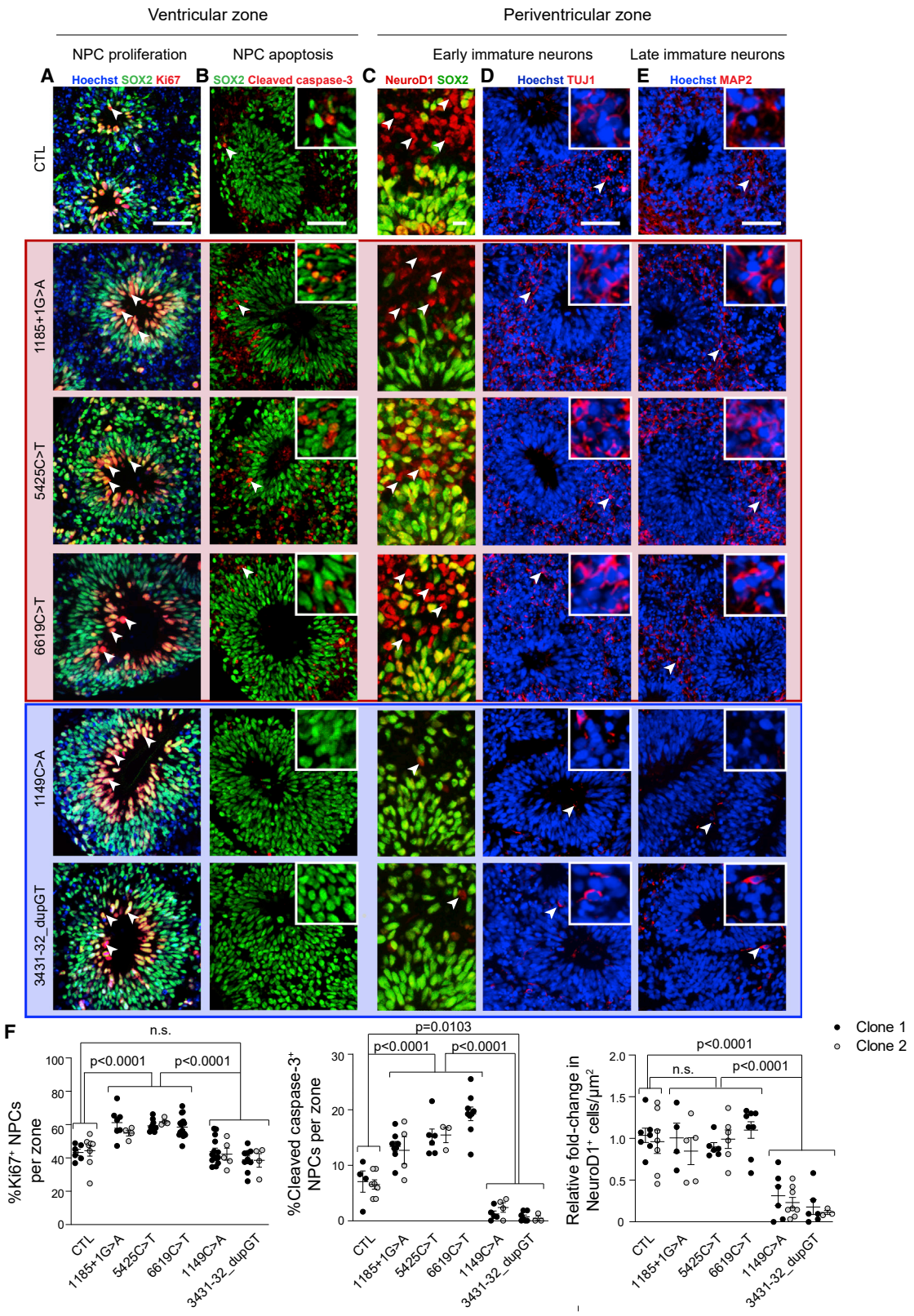

(legend on next page)

Conclusions

The findings described in this report, in combination with compelling population-based genotype-phenotype associations, suggest that the germline *NF1* gene mutation is one of the factors that underlies clinical heterogeneity in patients with NF1. Using an isogenic series of *NF1*-mutant hiPSC lines, we identified differential *NF1* mutational effects on human CNS cells and tissues. Importantly, unlike previous studies, the use of an isogenic series of hiPSCs eliminates other contributing factors, such as sex and genomic variation (potential modifier genes), and permits a direct examination of the effects of different *NF1* gene mutations. Moreover, this study raises several important points relevant to NF1 pathobiology.

First, we established that all heterozygous *NF1* gene mutations similarly increase CNS NPC and astroglial cell proliferation and RAS activity, which is consistent with numerous reports demonstrating that neurofibromin controls cell proliferation largely by regulating RAS activity in mouse, swine, and *Drosophila* cells and tissues. Moreover, the regulation of RAS-mediated cell proliferation by neurofibromin is further supported using paired hiPSC-derived NPCs, heterozygous and homozygous for the same *NF1* gene mutation, where a clear gene dose dependency was revealed (C. Anastasaki, Personal Communication). Therefore, the vast majority of human clinical trials for *NF1*-null tumors have appropriately used molecularly targeted therapies that inhibit RAS and RAS downstream effectors (e.g., MEK) (Dombi et al., 2016).

Second, we demonstrated differential effects of *NF1* germline mutations on neuronal differentiation. These differential effects could reflect the fact that neurofibromin functions as a high-affinity dimer, where different mutations could change the overall architecture of the dimer interface (Sherekar et al., 2020). Because neurons from individuals with NF1 harbor only a single *NF1* germline mutation, different *NF1* mutations likely cause unique neuron-related pathologies. Therefore, the use of isogenic hiPSCs revealed differential effects of distinct *NF1* gene mutations on NPC proliferation, apoptosis, and neuronal differentiation not previously reported in the developing *Nf1*-knockout ($Nf1^{wt/neo}$) mouse brain. Given the high degree of mutational specificity for autism symptomatology in children with NF1 (Morris and Gutmann, 2018), these findings suggest that investigations using *Nf1* mice with different patient germline *Nf1* mutations might uncover unique behavioral abnormalities not appreciated using conventional *Nf1* knockout mice (Costa et al., 2002; Omrani et al., 2015) and identify causative underlying molecular mechanisms.

Third, the fact that the observed differences in neuronal differentiation in cerebral organoids and NPC DA levels do not correlate with RAS activation supports the existence of non-RAS-mediated neurofibromin functions. In this regard, neurofibromin also directly binds to several proteins important for neuronal differentiation, spinogenesis, and serotonin receptor activity, including collapsin response mediator protein-2 (Patrakitkomjorn et al., 2008), syndecan (Hsueh et al., 2001), and the 5-hydroxyltryptamine-6 receptor (Deraredj Nadim et al., 2016), through domains distinct from the GRD. Moreover, the notion that non-RAS-mediated neurofibromin functions exist in neurons is reinforced by the presence of a neurofibromin isoform containing an additional amino terminal exon (11alt12), whose expression is restricted to postnatal brain neurons (Gutmann et al., 1999). Future investigations aimed at discovering novel neuron-specific neurofibromin binding partners will be critical to understanding how *NF1* mutations differentially affect cognition and behavior in children with NF1.

Finally, although population and murine studies provided the first evidence for *NF1* genotype-phenotype correlations, there had been no direct demonstration of the primary effect of the *NF1* mutation at the cellular and tissue levels in humans. The use of this experimental human iPSC platform revealed *NF1* mutational abnormalities in human NPCs and neurons. Collectively, these studies establish a foundational basis for future studies aimed at unraveling mechanistic etiologies responsible for *NF1*-specific CNS phenotypes, discovering new therapeutic targets, and assessing treatments relevant to precision medicine.

Figure 4. Differential Effects of *NF1* Mutations on Cerebral Organoid Progenitor Cell Dynamics and Neurogenesis

(A and B) $SOX2^+$ NPCs in the ventricular zones of group 1 *NF1*-mutant cerebral organoids exhibit (A) 1.3- to 1.4-fold increased proliferation ($Ki67^+$ cells; white arrowheads) and (B) 2- to 3-fold increased cell apoptosis (cleaved caspase-3; white arrowheads) compared with control and group 2 cerebral organoids at 16 DIV.

(C–E) Decreased numbers of (C and D) early immature neurons (NeuroD1; TUJ1 white arrowheads) and (E) late immature neurons (MAP2; white arrowheads) migrating into the periventricular zone of group 2 compared with group 1 and control cerebral organoids at 16 DIV.

(F) Quantifications of $\%Ki67^+$ NPCs, %cleaved caspase-3^+ NPCs and $NeuroD1^+$ immature neurons in *NF1*-mutant cerebral organoids compared with controls at 16 DIV.

Each dot represents an independently generated data point derived from separate experiments and the two different clones for each line are denoted as black versus gray dots. All data are represented as means ± SEM. One-way ANOVA with Dunnett post-test. n.s., not significant. Scale bars, 10 μm (C) and 50 μm (A, B, D, and E).

EXPERIMENTAL PROCEDURES

Human iPSCs

Seven distinct NF1-patient germline *NF1* gene mutations (Transcript ID NM_000267; c.1149C > A, c.1185+1G > A, c.2041C > T, c.3431-32_dupGT, c.5425C > T, c.6513T > A, c.6619C > T) were individually engineered using CRISPR/Cas9 technology into a single commercially available male control human iPSC line (BJFF.6) by the Washington University Genome Engineering and iPSC Core (GEiC) facility. Heterozygous mutations were confirmed by NGS sequencing (Bell et al., 2014), and two different clones were expanded for each of the six *NF1*-mutant and the control lines (Figures S1A–S1C). Only a single clone heterozygous for the c.6619C > T *NF1* mutation could be generated without any additional genomic insertions or deletions. Retention of heterozygosity in the hiPSCs was confirmed by sequencing after five passages, as well as in all of the derivative cell lines by RAS activity assays. Similar results were obtained after each passage. In addition, iPSCs reprogrammed from the fibroblasts of three NF1 patients (c.1185+1G > A; c.5425C > T; c.6513T > A) and one control subject (Anastasaki et al., 2015) were used for subsequent analyses. For NPC differentiation, hiPSCs were passaged onto PLO/Laminin (Millipore Sigma)-coated plates using ReLeSR (STEMCELL Technologies), and seeded at 200,000 cells/cm^2 in NPC induction medium (50% DMEM F12 [Gibco], 50% Neurobasal medium [Gibco], supplemented with N2, B27 [Fisher], 2 mM GlutaMAX [Gibco], 10 ng/mL hLIF, 4 μM CHIR99021, 3 μM SB431541, and 0.1 μM Compound E [all from STEMCELL Technologies]). Cells were maintained in this medium supplemented with 2 μM dorsomorphin for 3 days and without dorsomorphin (STEMCELL Technologies) for an additional 5 days. NPCs were subsequently incubated in NPC maturation medium (50% DMEM/F12, 50% Neurobasal medium supplemented with N2, B27, 2 mM GlutaMAX, 10 ng/mL hLIF, 3 μM CHIR99021 and 2 μM SB431541), and were passaged weekly following Accutase (STEMCELL Technologies) dissociation according to the manufacturer's instructions. NPCs were treated for 24 h with 10 μg/μL of FGF or BDNF (both STEMCELL Technologies) to assess growth factor-induced cell proliferation. GABAergic neurons were differentiated as described previously (Liu et al., 2013). For astrocytic differentiation, NPCs were plated on Primaria-coated plates in Astrocyte Growth Media (ScienCell) for a minimum of 2 weeks and a maximum of ten passages (Tcw et al., 2017). Cerebral organoids were generated as described previously (Lancaster and Knoblich, 2014) with minor modifications: embryoid bodies were cultured in NIM (STEMCELL Technologies) supplemented with 20 μM Rock inhibitor Y27632 (Millipore) and 4 ng/mL basic FGF (Peprotech) for the first 5 days, followed by NIM alone for an additional 4 days, before direct transfer to cerebral organoid media without Matrigel embedding. Cerebral organoids were maintained for up to 56 DIV. All experiments used at least three biological replicates from two independently generated hiPSC clones.

RNA Extraction, cDNA Production, qPCR, and Targeted Allele Expression Analysis

Total RNA was extracted from snap-frozen cell pellets of three independent passages of two clones per hiPSC line, using QIAGEN RNeasy Mini Kit. Total RNA was reverse-transcribed into cDNA using an Applied Biosystems High-Capacity cDNA Reverse Transcription Kit as per the manufacturer's instructions. Real-time quantitative PCR (qPCR) was performed using TaqMan Gene Expression assays *NF1* (Hs01035108_m1) and *GAPDH* (Hs02786624_g1; internal control), and relative *NF1* expression was calculated using the ΔΔCT analysis method following the manufacturer's instructions (Thermo Fisher Scientific). For allele-specific expression analyses, primer pairs including Illumina adapter sequences concatenated to their 5′ ends were used for all *NF1*-mutant hiPSCs to initially amplify the mutation-surrounding region, and later to add the P5 sites, P7 sites, and sample-specific index (Supplemental Experimental Procedures). The samples were pooled and the amplicons were deep-sequenced on a MiSeq machine. Illumina adapters, 5′ and 3′ bases with quality scores <25, as well as sequences <25 bases long were trimmed using Trimmomatic v.0.331 software. Trimmed reads were aligned to the human reference genome hg19 using STARv2.52 software and allele reads were calculated using Integrative Genomics Viewer v.2.3.293.

Immunohistochemistry and ELISA Assays

Immunocytochemistry on NPCs, astrocytes, and neurons was performed following established protocols (Anastasaki et al., 2015) using the antibodies described (Table S2). RAS activity (Thermo Fisher Scientific), GABA, dopamine (both Rocky Mountain Diagnostics) detection (Anastasaki et al., 2015), BrdU proliferation assays (Roche), and direct cell counting were performed as described previously (Toonen et al., 2016). Immunohistochemistry on cryosections of cerebral organoids was performed as described previously (Sloan et al., 2018). A minimum of three independent samples representing different passages of two separate clones were used for each line.

Mice

All animals were maintained on an inbred C57BL/6 background using a 12-h light/dark cycle with *ad libitum* access to food and water. Heterozygous *Nf1* mice were generated to harbor point mutations corresponding to the human c.1149C > A, c.2041C > T, c.3431_32dupGT, and c.5425C > T mutations. The c.1149C > A, c.2041C > T, and c.3431_32dupGT mice were generated using C57BL/6 embryonic stem cells backcrossed a minimum of 10 times to wild-type C57BL/6 mice, while the c.5425C > T mice were generated by CRISPR/Cas9 engineering on a C57BL/6 genetic background and heterozygous mutation was confirmed by direct sequencing. All mice were used in accordance with an approved Animal Studies Protocol at the Washington University School of Medicine.

Statistics

All statistical tests were performed using GraphPad Prism 5 software. We performed t tests, one- or two-way analysis of variance (ANOVA) with Dunnett or Bonferroni post-test correction using GraphPad Prism 5 software. Statistical significance was set at $p < 0.05$.

ACCESSION NUMBERS

The accession number for the deep sequencing data reported in this paper is GEO: GSE144601.

SUPPLEMENTAL INFORMATION

Supplemental Information can be found online at https://doi.org/10.1016/j.stemcr.2020.03.007.

AUTHOR CONTRIBUTIONS

C.A., M.L.W., and D.H.G. designed and analyzed the experiments. C.A., M.L.W., K.H., J.B.P., N.D.K., J.C., O.C., and J.D.D. conducted and/or interpreted the experiments. The article was assembled by C.A., M.L.W., and D.H.G. D.H.G. was responsible for the final production of the manuscript.

ACKNOWLEDGMENTS

This work was supported by an R50 Research Specialist Award from the National Cancer Institute, USA (1-R50-CA233164-01 to C.A.), a Young Investigator's Award grant from the Children's Tumor Foundation, USA (2018-01-003 to M.L.W.), and a Research Program Award grant from the National Insitute of Neurological Disorders and Stroke, USA (1-R35-NS07211-01 to D.H.G.). The GEiC Center at WUSM engineered the hiPSCs and is subsidized by National Cancer Institute, USA Cancer Center Support grant (P30-CA091842). Dr. Gutmann has a licensing agreement for the GFAP-Cre mouse strain with the Tuberous Sclerosis Alliance.

Received: April 19, 2019
Revised: March 5, 2020
Accepted: March 6, 2020
Published: April 2, 2020

REFERENCES

Anastasaki, C., Morris, S.M., Gao, F., and Gutmann, D.H. (2017). Children with 5′-end NF1 gene mutations are more likely to have glioma. Neurol. Genet. *3*, e192.

Anastasaki, C., Woo, A.S., Messiaen, L.M., and Gutmann, D.H. (2015). Elucidating the impact of neurofibromatosis-1 germline mutations on neurofibromin function and dopamine-based learning. Hum. Mol. Genet. *24*, 3518–3528.

Bell, C.C., Magor, G.W., Gillinder, K.R., and Perkins, A.C. (2014). A high-throughput screening strategy for detecting CRISPR-Cas9 induced mutations using next-generation sequencing. BMC Genomics *15*, 1002.

Bolcekova, A., Nemethova, M., Zatkova, A., Hlinkova, K., Pozgayova, S., Hlavata, A., Kadasi, L., Durovcikova, D., Gerinec, A., Husakova, K., et al. (2013). Clustering of mutations in the 5′ tertile of the NF1 gene in Slovakia patients with optic pathway glioma. Neoplasma *60*, 655–665.

Costa, R.M., Federov, N.B., Kogan, J.H., Murphy, G.G., Stern, J., Ohno, M., Kucherlapati, R., Jacks, T., and Silva, A.J. (2002). Mechanism for the learning deficits in a mouse model of neurofibromatosis type 1. Nature *415*, 526–530.

Cui, Y., Costa, R.M., Murphy, G.G., Elgersma, Y., Zhu, Y., Gutmann, D.H., Parada, L.F., Mody, I., and Silva, A.J. (2008). Neurofibromin regulation of ERK signaling modulates GABA release and learning. Cell *135*, 549–560.

Deraredj Nadim, W., Chaumont-Dubel, S., Madouri, F., Cobret, L., De Tauzia, M.L., Zajdel, P., Benedetti, H., Marin, P., and Morisset-Lopez, S. (2016). Physical interaction between neurofibromin and serotonin 5-HT6 receptor promotes receptor constitutive activity. Proc. Natl. Acad. Sci. U S A *113*, 12310–12315.

Dombi, E., Baldwin, A., Marcus, L.J., Fisher, M.J., Weiss, B., Kim, A., Whitcomb, P., Martin, S., Aschbacher-Smith, L.E., Rizvi, T.A., et al. (2016). Activity of selumetinib in neurofibromatosis type 1-related plexiform neurofibromas. N. Engl. J. Med. *375*, 2550–2560.

Fisher, M.J., Belzberg, A.J., de Blank, P., De Raedt, T., Elefteriou, F., Ferner, R.E., Giovannini, M., Harris, G.J., Kalamarides, M., Karajannis, M.A., et al. (2018). 2016 Children's Tumor Foundation conference on neurofibromatosis type 1, neurofibromatosis type 2, and schwannomatosis. Am. J. Med. Genet. A *176*, 1258–1269.

Gutmann, D.H., Zhang, Y., and Hirbe, A. (1999). Developmental regulation of a neuron-specific neurofibromatosis 1 isoform. Ann. Neurol. *46*, 777–782.

Hsueh, Y.P., Roberts, A.M., Volta, M., Sheng, M., and Roberts, R.G. (2001). Bipartite interaction between neurofibromatosis type I protein (neurofibromin) and syndecan transmembrane heparan sulfate proteoglycans. J. Neurosci. *21*, 3764–3770.

Hyman, S.L., Shores, A., and North, K.N. (2005). The nature and frequency of cognitive deficits in children with neurofibromatosis type 1. Neurology *65*, 1037–1044.

Hyman, S.L., Arthur Shores, E., and North, K.N. (2006). Learning disabilities in children with neurofibromatosis type 1: subtypes, cognitive profile, and attention-deficit-hyperactivity disorder. Dev. Med. Child Neurol. *48*, 973–977.

Jett, K., and Friedman, J.M. (2010). Clinical and genetic aspects of neurofibromatosis 1. Genet. Med. *12*, 1–11.

Kehrer-Sawatzki, H., Mautner, V.F., and Cooper, D.N. (2017). Emerging genotype-phenotype relationships in patients with large NF1 deletions. Hum. Genet. *136*, 349–376.

Koczkowska, M., Callens, T., Gomes, A., Sharp, A., Chen, Y., Hicks, A.D., Aylsworth, A.S., Azizi, A.A., Basel, D.G., Bellus, G., et al. (2018). Expanding the clinical phenotype of individuals with a 3-bp in-frame deletion of the NF1 gene (c.2970_2972del): an update of genotype-phenotype correlation. Genet. Med. *21*, 867–876.

Korf, B.R. (2013). Neurofibromatosis. Handb. Clin. Neurol. *111*, 333–340.

Lancaster, M.A., and Knoblich, J.A. (2014). Generation of cerebral organoids from human pluripotent stem cells. Nat. Protoc. *9*, 2329–2340.

Liu, Y., Liu, H., Sauvey, C., Yao, L., Zarnowska, E.D., and Zhang, S.C. (2013). Directed differentiation of forebrain GABA interneurons from human pluripotent stem cells. Nat. Protoc. *8*, 1670–1679.

Morris, S.M., and Gutmann, D.H. (2018). A genotype-phenotype correlation for quantitative autistic trait burden in neurofibromatosis 1. Neurology *90*, 377–379.

Omrani, A., van der Vaart, T., Mientjes, E., van Woerden, G.M., Hojjati, M.R., Li, K.W., Gutmann, D.H., Levelt, C.N., Smit, A.B., Silva, A.J., et al. (2015). HCN channels are a novel therapeutic target for cognitive dysfunction in neurofibromatosis type 1. Mol. Psychiatry *20*, 1311–1321.

Patrakitkomjorn, S., Kobayashi, D., Morikawa, T., Wilson, M.M., Tsubota, N., Irie, A., Ozawa, T., Aoki, M., Arimura, N., Kaibuchi, K., et al. (2008). Neurofibromatosis type 1 (NF1) tumor suppressor, neurofibromin, regulates the neuronal differentiation of PC12 cells via its associating protein, CRMP-2. J. Biol. Chem. *283*, 9399–9413.

Pinna, V., Lanari, V., Daniele, P., Consoli, F., Agolini, E., Margiotti, K., Bottillo, I., Torrente, I., Bruselles, A., Fusilli, C., et al. (2015). p.Arg1809Cys substitution in neurofibromin is associated with a distinctive NF1 phenotype without neurofibromas. Eur. J. Hum. Genet. *23*, 1068–1071.

Rojnueangnit, K., Xie, J., Gomes, A., Sharp, A., Callens, T., Chen, Y., Liu, Y., Cochran, M., Abbott, M.A., Atkin, J., et al. (2015). High incidence of Noonan syndrome features including short stature and pulmonic stenosis in patients carrying NF1 missense mutations affecting p.Arg1809: genotype-phenotype correlation. Hum. Mutat. *36*, 1052–1063.

Sharif, S., Upadhyaya, M., Ferner, R., Majounie, E., Shenton, A., Baser, M., Thakker, N., and Evans, D.G. (2011). A molecular analysis of individuals with neurofibromatosis type 1 (NF1) and optic pathway gliomas (OPGs), and an assessment of genotype-phenotype correlations. J. Med. Genet. *48*, 256–260.

Sherekar, M., Han, S.W., Ghirlando, R., Messing, S., Drew, M., Rabara, D., Waybright, T., Juneja, P., O'Neill, H., Stanley, C.B., et al. (2020). Biochemical and structural analyses reveal that the tumor suppressor neurofibromin (NF1) forms a high-affinity dimer. J. Biol. Chem. *295*, 1105–1119.

Sloan, S.A., Andersen, J., Pasca, A.M., Birey, F., and Pasca, S.P. (2018). Generation and assembly of human brain region-specific three-dimensional cultures. Nat. Protoc. *13*, 2062–2085.

Tcw, J., Wang, M., Pimenova, A.A., Bowles, K.R., Hartley, B.J., Lacin, E., Machlovi, S.I., Abdelaal, R., Karch, C.M., Phatnani, H., et al. (2017). An efficient platform for astrocyte differentiation from human induced pluripotent stem cells. Stem Cell Reports *9*, 600–614.

Toonen, J.A., Anastasaki, C., Smithson, L.J., Gianino, S.M., Li, K., Kesterson, R.A., and Gutmann, D.H. (2016). NF1 germline mutation differentially dictates optic glioma formation and growth in neurofibromatosis-1. Hum. Mol. Genet. *25*, 1703–1713.

Trevisson, E., Morbidoni, V., Forzan, M., Daolio, C., Fumini, V., Parrozzani, R., Cassina, M., Midena, E., Salviati, L., and Clementi, M. (2019). The Arg1038Gly missense variant in the NF1 gene causes a mild phenotype without neurofibromas. Mol. Genet. Genomic Med. *7*, e616.

Upadhyaya, M., Huson, S.M., Davies, M., Thomas, N., Chuzhanova, N., Giovannini, S., Evans, D.G., Howard, E., Kerr, B., Griffiths, S., et al. (2007). An absence of cutaneous neurofibromas associated with a 3-bp inframe deletion in exon 17 of the NF1 gene (c.2970-2972 delAAT): evidence of a clinically significant NF1 genotype-phenotype correlation. Am. J. Hum. Genet. *80*, 140–151.

Stem Cell Reports, Volume *14*

Supplemental Information

Human iPSC-Derived Neurons and Cerebral Organoids Establish Differential Effects of Germline *NF1* Gene Mutations

Corina Anastasaki, Michelle L. Wegscheid, Kelly Hartigan, Jason B. Papke, Nathan D. Kopp, Jiayang Chen, Olivia Cobb, Joseph D. Dougherty, and David H. Gutmann

Supplementary Figures

Figure S1. Isogenic *NF1*-mutant hiPSC sequencing and allele expression analysis of isogenic and patient-derived *NF1*-mutant hiPSCs.

Figure S2. Analysis of isogenic hiPSCs, NPCs, and cerebral organoids.

Figure S3. Comparisons between isogenic and patient-derived *NF1*-mutant hiPSC-NPCs.

Figure S4. Comparisons between isogenic and patient-derived *NF1*-mutant hiPSC-organoids.

Table S1. Inter-clone analysis of control and *NF1*-mutant hiPSC-derived cells and organoids.

Table S2. Primary antibodies used.

Supplementary Methods

Figure S1. Isogenic *NF1*-mutant hiPSC sequencing and allele expression analysis of isogenic and patient-derived *NF1*-mutant hiPSCs.

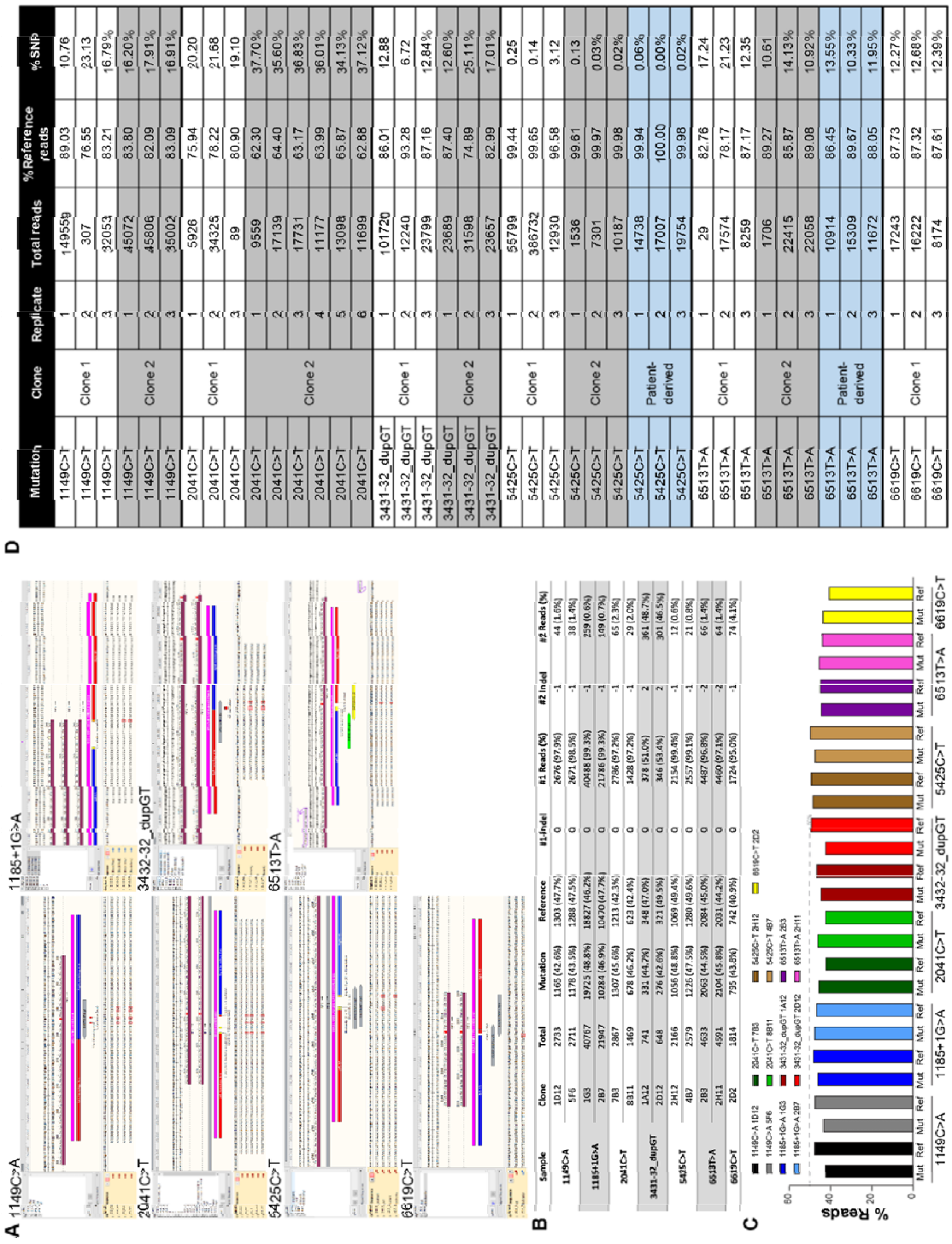

Mutation	Clone	Replicate	Total reads	% Reference reads	% SNP
1149C>T	Clone 1	1	149559	89.03	10.76
1149C>T		2	307	76.55	23.13
1149C>T		3	32053	83.21	16.79%
1149C>T	Clone 2	1	45072	83.80	16.20%
1149C>T		2	45806	82.09	17.91%
1149C>T		3	35002	83.09	16.91%
2041C>T	Clone 1	1	5926	75.94	20.20
2041C>T		2	34325	78.22	21.68
2041C>T		3	89	80.90	19.10
2041C>T	Clone 2	1	9559	62.30	37.70%
2041C>T		2	17139	64.40	35.60%
2041C>T		3	17731	63.17	36.83%
2041C>T		4	11177	63.99	36.01%
2041C>T		5	13098	65.87	34.13%
2041C>T		6	11699	62.88	37.12%
3431-32_dupGT	Clone 1	1	101720	86.01	12.88
3431-32_dupGT		2	12240	93.28	6.72
3431-32_dupGT		3	23799	87.16	12.84%
3431-32_dupGT	Clone 2	1	23689	87.40	12.60%
3431-32_dupGT		2	31598	74.89	25.11%
3431-32_dupGT		3	23657	82.99	17.01%
5425C>T	Clone 1	1	55799	99.44	0.25
5425C>T		2	386732	99.65	0.14
5425C>T		3	12930	96.58	3.12
5425C>T	Clone 2	1	1536	99.61	0.13
5425C>T		2	7301	99.97	0.03%
5425C>T		3	10187	99.98	0.02%
5425C>T	Patient-derived	1	14738	99.94	0.06%
5425C>T		2	17007	100.00	0.00%
5425C>T		3	19754	99.98	0.02%
6513T>A	Clone 1	1	29	82.76	17.24
6513T>A		2	17574	78.17	21.23
6513T>A		3	8259	87.17	12.35
6513T>A	Clone 2	1	1706	89.27	10.61
6513T>A		2	22415	85.87	14.13%
6513T>A		3	22058	89.08	10.92%
6513T>A	Patient-derived	1	10914	86.45	13.55%
6513T>A		2	15309	89.67	10.33%
6513T>A		3	11672	88.05	11.95%
6619C>T	Clone 1	1	17243	87.73	12.27%
6619C>T		2	16222	87.32	12.68%
6619C>T		3	8174	87.61	12.39%

Figure S1. Sequencing of *NF1*-mutant hiPSCs. (**A**) Snapgene view of NGS sequencing of all *NF1*-mutant hiPSC clones. (Block only: control; Block/mod: introduced *NF1* gene mutation). (**B-C**) Table and histogram summarizing the percentage of sequence reads detected for the mutant and reference (wild-type) alleles at the mutation site at the genomic level. (**D**) Analysis of reference and mutant (SNP) allele expression in each *NF1*-mutant hiPSC line at the RNA level demonstrates that the wild-type reference allele is over-represented in all *NF1*-mutant hiPSCs relative to the mutation-bearing (SNP) allele. Data are represented as the percentages of reference and mutant reads relative to the total reads.

Figure S2. Analysis of isogenic hiPSCs, NPCs, and cerebral organoids.

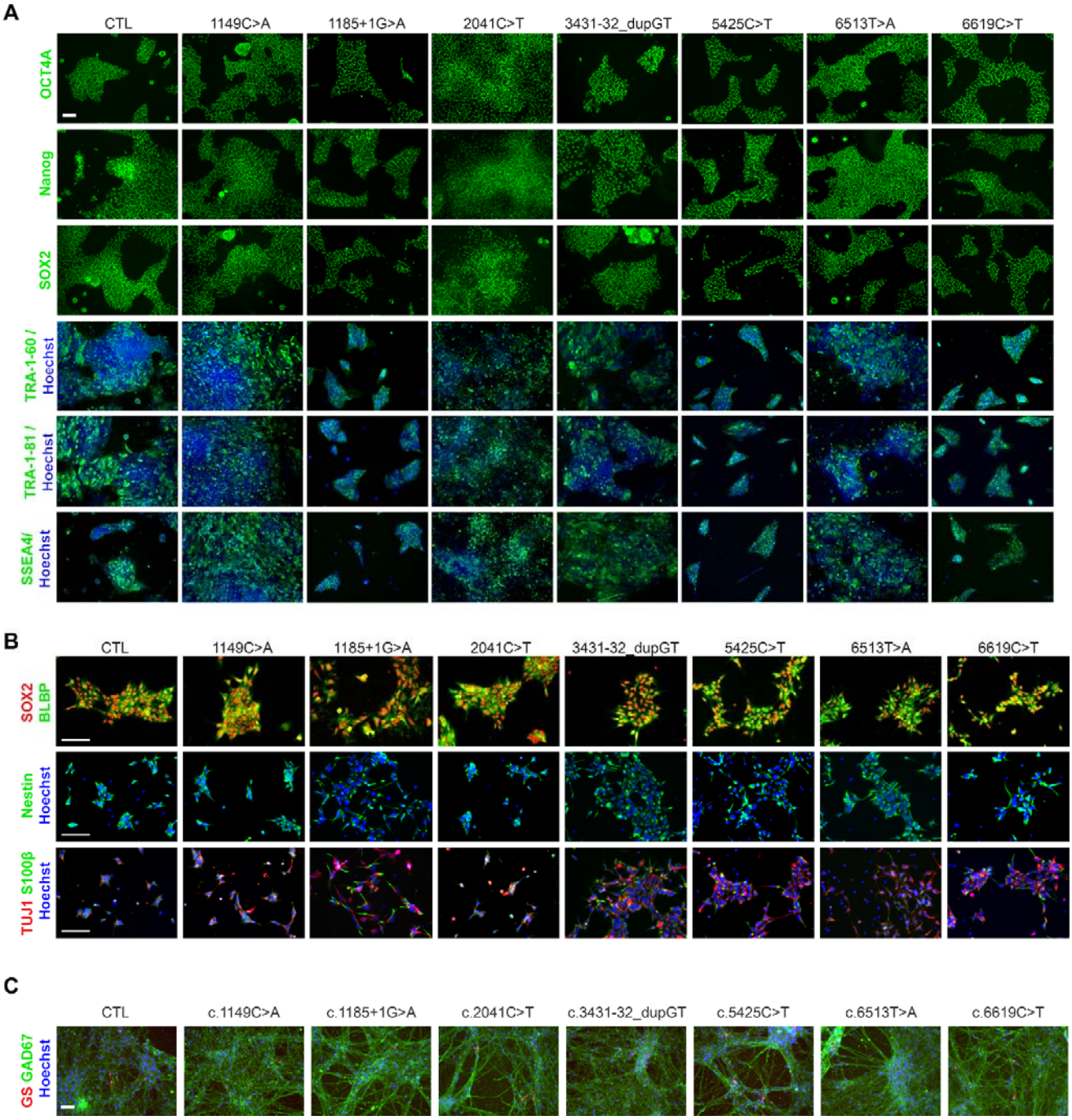

Figure S2. (**A**) Immunofluorescence analysis of all hiPSCs with the NANOG, SOX2, OCT4A, SSEA-4, TRA-1-60, and TRA-1-81 pluripotency markers. Scale bar, 100μm. (**B**) NPCs were

immunopositive for the SOX2, BLBP and Nestin neural stem cell markers (top two panels), and were multipotent, as illustrated by $TUJ1^+$ and $S100\beta^+$ double labeling (bottom panel). Scale bars, 100μm. (**C**) Control and *NF1*-mutant NPC-differentiated GABAergic neuronal cultures were immunopositive for GAD67 (green) and immunonegative for the excitatory neuron marker glutamate synthetase (GS; red). Scale bar, 100μm.

Figure S3. Comparisons between isogenic and patient-derived *NF1*-mutant hiPSC-NPCs.

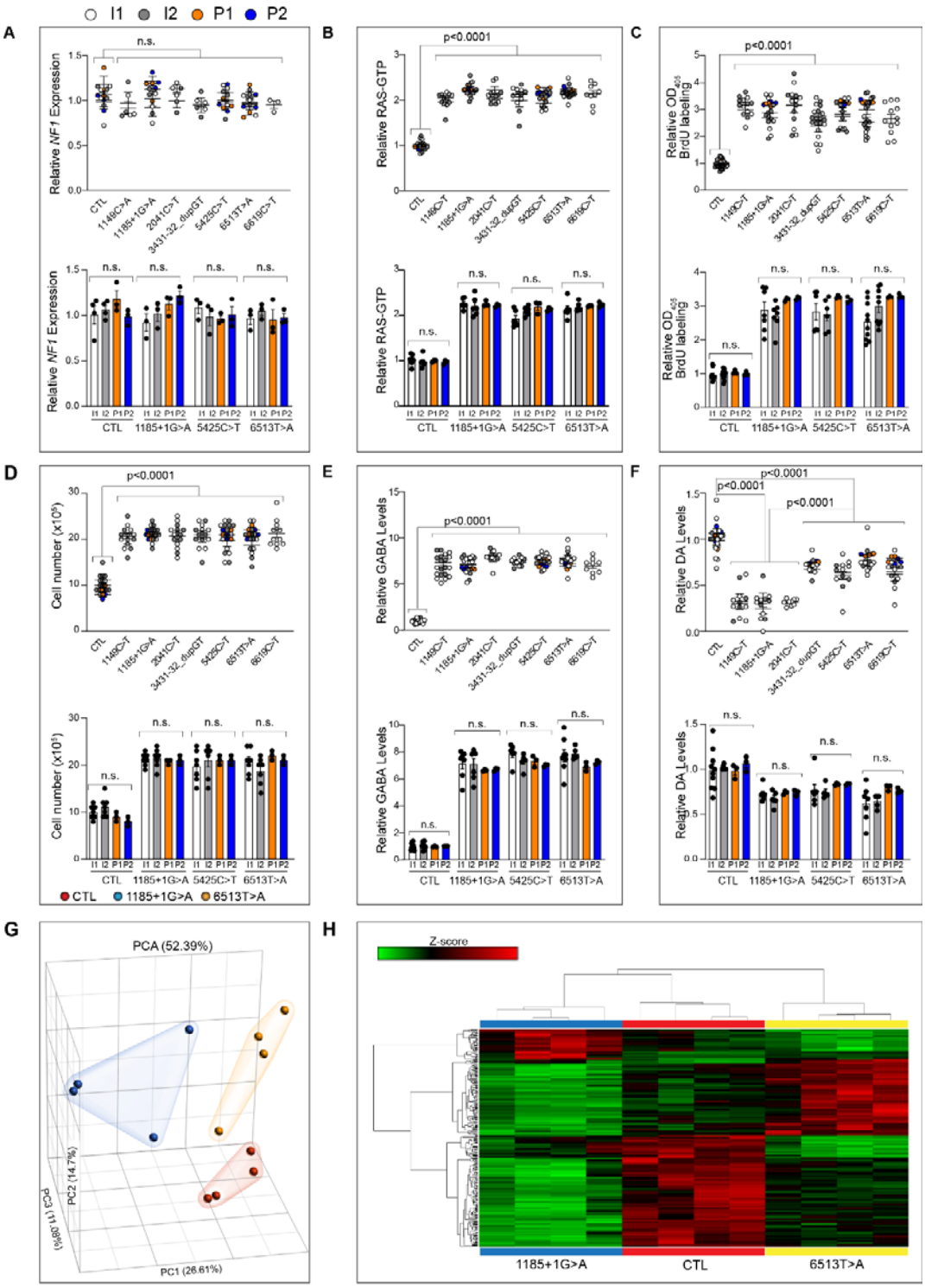

Figure S3. (**A**) Relative *NF1* mRNA expression, (**B**) RAS activity, (**C**) BrdU incorporation, and (**D**) cell numbers are similar between the isogenic and their respective patient-derived NPC lines that harbor the same *NF1* gene mutation. The top panels illustrate all the clones (Isogenic clones: I1, I2; white, grey circles, respectively; Patient-derived clones: P1, P2; orange and blue circles, respectively) employed for each assay, and represent comparisons between all *NF1*-mutant NPCs and controls. The bottom panels illustrate the individual comparisons between the isogenic (I1, I2) and their respective patient-derived (P1, P2) NPCs (CTL; 1185+1G>A; 5425C>T; 6513T>A). Relative (**E**) GABA levels and (**F**) DA levels are similar between the isogenic and their respective patient-derived NPC lines harboring the same *NF1* gene mutation. The top panels illustrate all the clones (Isogenic clones: I1, I2; white, grey circles, respectively; Patient-derived clones: P1, P2; orange and blue circles, respectively) employed for each assay, and represent the comparisons between all *NF1*-mutant NPCs and controls. The bottom panels illustrate the individual comparisons between the isogenic (I1, I2) and their respective patient-derived (P1, P2) NPCs (CTL; 1185+1G>A; 5425C>T; 6513T>A). All data are represented as means ± SEM; One-way ANOVA with Tukey post-test. ns, not significant. (**G**) PCA plot and (**H**) histogram analysis illustrate differential clustering of gene expression between patient-derived and isogenic NPCs harboring two separate *NF1* mutations (1185+1G>A; 6513T>A) or no *NF1* mutation (control; CTL), following next-generation sequencing.

Figure S4. Comparisons between isogenic and patient-derived *NF1*-mutant hiPSC-organoids.

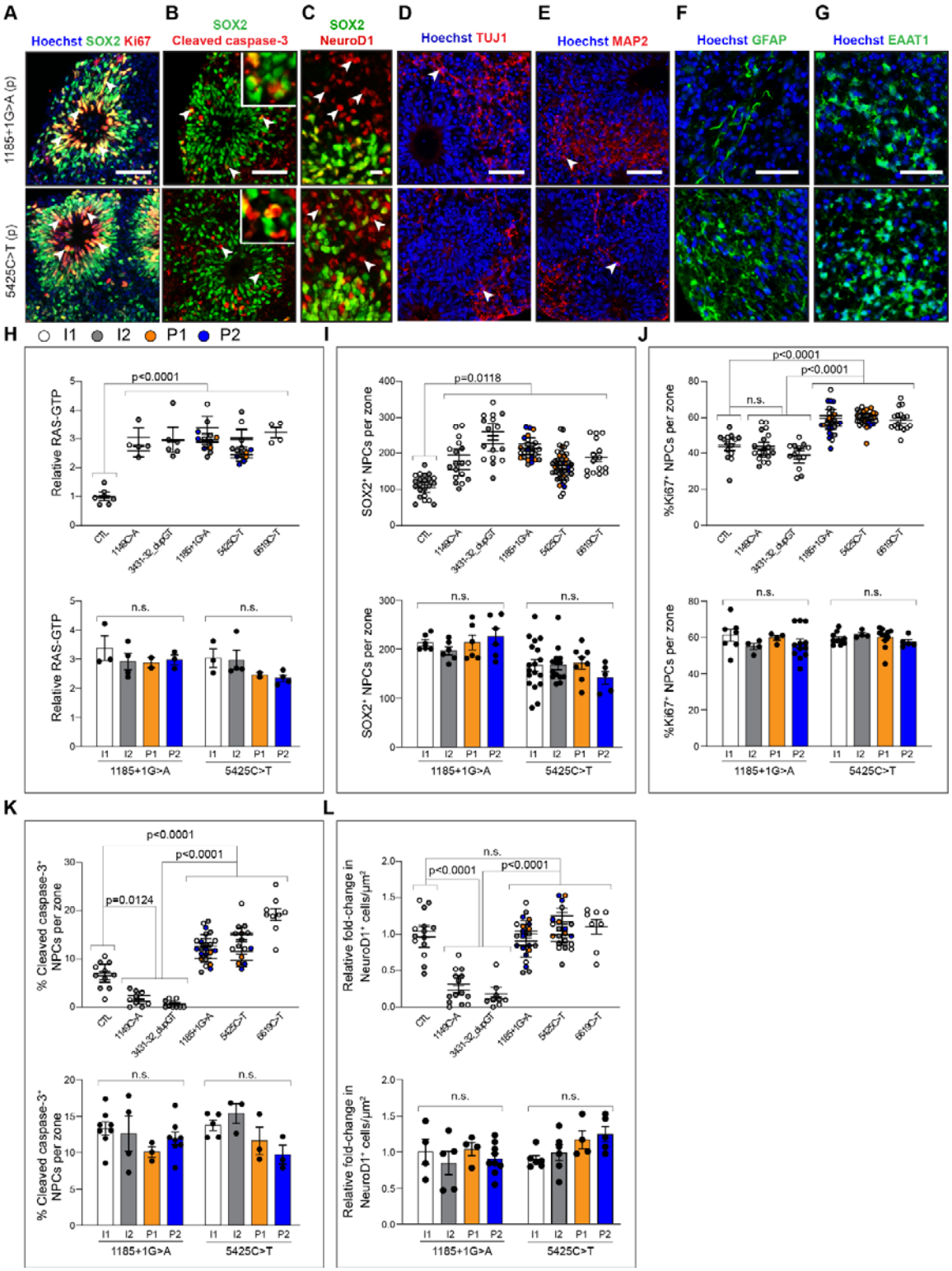

Figure S4. Representative images of (**A**) NPC proliferation (Ki67$^+$ cells; white arrowheads), (**B**) NPC apoptosis (cleaved caspase-3; white arrowheads), (**C, D**) early immature neurons (NeuroD1; TUJ1; white arrowheads), (**E**) late immature neurons (MAP2; white arrowheads) at 16DIV, and the production of (**F**) EAAT1$^+$ glial cells and (**G**) GFAP$^+$ fibers at 56DIV in cerebral organoids generated from 1185+1G>A and 5425C>T patient-derived hiPSC lines. Scale bars: (**C**) 10μm, (**A, B, D, E, F, G**) 50μm. There were no differences in (**H**) RAS activity or (**I**) SOX2$^+$ NPCs per ventricular zone (VZ) between the isogenic *NF1*-mutant cerebral organoids and their corresponding patient-derived at 16DIV. There were no differences in (**J**) %Ki67$^+$ NPCs per VZ, (K) %cleaved caspase-3$^+$ NPCs per VZ, or (**L**) NeuroD1$^+$ immature neurons between the isogenic *NF1*-mutant and their corresponding patient-derived cerebral organoids at 16DIV. The top panels illustrate all the clones (Isogenic clones: I1, I2; white, grey circles, respectively; Patient-derived clones: P1, P2; orange and blue circles, respectively) employed for each assay, and represent the comparisons between all *NF1*-mutant organoids and controls. The bottom panels illustrate the individual comparisons between the isogenic (I1, I2) and their respective patient-derived (P1, P2) NPCs (1185+1G>A; 5425C>T). All data are represented as means ± SEM; One-way ANOVA with Tukey post-test. ns, not significant.

Table S1. Inter-clone analysis of control and *NF1*-mutant hiPSC-derived cells and organoids.

	NPCs *NF1* Relative Expression		Isogenic NPCs *			Isogenic Astrocytes *		
	Isogenic *	Isogenic vs Patient-derived **	RAS assays	BrdU Assays	Direct cell count	RAS assays	BrdU Assays	Direct cell count
CTL	0.598	0.479 / 0.634	0.559	0.929	0.258	0.317	0.566	0.775
1149C>T	0.153	n/a	0.383	0.155	0.657	0.604	0.395	0.690
1185+1G>A	0.953	0.046 / 0.956	0.564	0.552	0.758	0.532	0.504	0.563
2041C>T	0.381	n/a	0.078	0.939	>0.999	0.847	0.543	0.142
3431-32_dupGT	0.570	n/a	0.363	0.146	0.686	0.709	0.426	0.553
5425C>T	0.151	3.380 / 0.104	0.065	0.785	0.491	0.742	0.458	0.060
6513T>A	0.846	0.941 / 0.441	0.590	0.093	0.204	0.148	0.096	>0.999

	Isogenic vs Patient-derived NPCs **			NPCs GABA		NPCs DA	
	RAS assays	BrdU Assays	Direct cell count	Isogenic *	Isogenic vs Patient-derived **	Isogenic *	Isogenic vs Patient-derived **
CTL	0.309 / 0.742	0.593 / 0.573	1.207 / 0.343	0.598	0.479 / 0.634	0.121	0.925 / 0.431
1149C>T	n/a	n/a	n/a	0.153	n/a	0.716	n/a
1185+1G>A	0.372 / 0.704	1.399 / 0.318	2.600 / 0.154	0.953	0.046 / 0.956	0.371	0.017 / 0.984
2041C>T	n/a	n/a	n/a	0.381	n/a	0.963	n/a
3431-32_dupGT	n/a	n/a	n/a	0.570	n/a	0.879	n/a
5425C>T	0.598 / 0.580	1.058 / 0.404	1.000 / 0.422	0.151	3.380 / 0.104	0.766	0.188 / 0.833
6513T>A	1.289 / 0.322	3.975 / 0.058	0.500 / 0.622	0.846	0.941 / 0.441	0.469	0.986 / 0.410

	Isogenic Organoids *					Isogenic vs Patient-derived **				
	Ki67$^+$	RAS assays	NSCs per PZ	NeuroD1$^+$	Cleaved Caspase 3$^+$	Ki67$^+$	RAS assays	NSCs per PZ	NeuroD1$^+$	Cleaved Caspase 3$^+$
CTL	0.803	0.943	0.367	0.651	0.603	n/a	n/a	n/a	n/a	n/a
1149C>T	0.711	0.354	0.125	0.517	0.433	n/a	n/a	n/a	n/a	n/a
1185+1G>A	0.217	0.383	0.138	0.527	0.784	0.830/ 0.491	0.561/ 0.656	0.632/ 0.599	0.488/ 0.695	0.838/ 0.491
3431-32_dupGT	0.944	0.951	0.291	0.636	0.895	n/a	n/a	n/a	n/a	n/a
5425C>T	0.216	0.909	0.982	0.466	0.288	0.780/ 0.516	1.850/ 0.208	0.632/ 0.599	2.675/ 0.080	4.029/ 0.037

Table S1. Table detailing the inter-clone analyses of isogenic iPSC-derived NPCs and organoids, as well as isogenic versus patient-derived hiPSC-derived NPCs and organoids harboring the same germline *NF1* mutations. There are no statistically significant differences in the relative *NF1* mRNA expression in NPCs, RAS activity, BrdU incorporation, or cell number in NPCs or astrocytes, GABA and dopamine (DA) levels in NPCs, %Ki67$^+$ progenitor cells per ventricular zone (VZ), RAS activity, NPCs per ventricular zone (VZ), NeuroD1$^+$ cells or %cleaved caspase-3$^+$ progenitor cells per VZ in cerebral organoids. *t-test; P-values reported, **One-Way ANOVA; F / P-values reported, respectively. n/a: not applicable.

Table S2. Primary antibodies used.

Antibody	Vendor	Catalog No	Host	Application (dilution)
BLBP	Millipore	ABN14	Rabbit	ICC (1:200)
Cleaved caspase-3	Cell Signaling	9664	Rabbit	IF (1:250)
EAAT1	Abcam	ab416	Rabbit	ICC, IF (1:500)
EAAT2	Abcam	ab41621	Rabbit	ICC (1:500)
GFAP	Abcam	ab4648	Mouse	ICC, IF (1:500)
Ki67	Fisher Scientific	BDB556003	Mouse	IF (1:100)
MAP2	Abcam	ab11267	Mouse	IF (1:500)
Nanog (D73G4)	Cell Signaling	9656S	Rabbit	ICC (1:200)
Nestin	Abcam	ab92391	Rabbit	ICC (1:250)
NeuroD1	Abcam	ab60704	Mouse	IF (1:500)
Oct-4A (C30A3)	Cell Signaling	9656S	Rabbit	ICC (1:200)
S100β	Abcam	ab41548	Rabbit	ICC (1:200)
SOX2	Cell Signaling	4900S	Mouse	ICC (1:1000); IF (1:250)
Sox2 (D6D9)	Cell Signaling	9656S	Rabbit	ICC (1:200)
SOX2	Abcam	ab92494	Rabbit	IF (1:250)
SSEA4 (MC813)	Cell Signaling	9656S	Mouse	ICC (1:200)
TRA-1-60(S)	Cell Signaling	9656S	Mouse	ICC (1:200)
TRA-1-81	Cell Signaling	9656S	Mouse	ICC (1:200)
TUJ-1	Abcam	ab78078	Mouse	ICC (1:1000)

Supplemental Methods

Next Generation RNA Sequencing and Analysis. RNA was extracted from three independently-generated samples of isogenic CTL or *NF1*-mutant (1185+1G>A; 6513T>A) NPCs, and one sample each from the non-isogenic CTL and patient-derived *NF1*-mutant NPCs harboring the same *NF1* mutations. Samples were prepared according to library kit manufacturer's protocol, indexed, pooled, and sequenced on an Illumina HiSeq. Basecalls and demultiplexing were performed with Illumina's bcl2fastq software and a custom python demultiplexing program with a maximum of one mismatch in the indexing read. RNA-seq reads were then aligned to the Ensembl release 76 primary assembly with STAR version 2.5.1a. Gene counts were derived from the number of uniquely aligned unambiguous reads by Subread:featureCount version 1.4.6-p5. Isoform expressions of known Ensembl transcripts were estimated with Salmon version 0.8.2. Sequencing performance was assessed for the total number of aligned reads, total number of uniquely aligned reads, and features detected. The ribosomal fraction, known junction saturation, and read distribution over known gene models were quantified with RSeQC version 2.6.2. The raw gene count matrix was then imported into Partek Flow software, version 8.0. Normalization size factors were calculated for all gene counts by CPM to adjust for differences in sequencing depth. Ribosomal genes and genes not expressed in the smallest group size minus samples greater than one count-per-million were excluded from further analysis. Gene-specific analysis was then performed using the lognormal with shrinkage model (limma-trend method) to analyze for differential expression between the three groups of samples. Principle component analysis (PCA) was conducted in Partek Flow using normalized gene counts. The "grouping" is simply a post hoc highlighting of the genotypes for assistance in visualizing that the different samples clustered together by genotype during the principle component. For further visualization, a heatmap was generated using the differential genes for each group filtered at p-values ≤ 0.05 and log fold-changes more extreme or equal to ±2.

Features and samples were clustered using Pearson Correlation as a distance metric. Deep sequencing data has been submitted to GEO with accession number GSE144601.

Allele-Specific Analysis Primers Used. The primers used for the first PCR reaction including the Illumina adaptor sequences were the following:

1149C>A FW: GTGACTGGAGTTCAGACGTGTGCTCTTCCGATCTCTACTTGTTCAGTCCATGGTGG

1149C>A REV: ACACTCTTTCCCTACACGACGCTCTTCCGATCTCCAATGCGGAATTGGTGATGA

2041C>T FW: GTGACTGGAGTTCAGACGTGTGCTCTTCCGATCTAATTACTACGTACTCCTGGAGC

2041C>T REV: ACACTCTTTCCCTACACGACGCTCTTCCGATCTGCAAGAGGTTATGCACTGAC

3431-32_dupGT FW: GTGACTGGAGTTCAGACGTGTGCTCTTCCGATCTGACTGCAGTGAAGTTGA AGATG

3431-32_dupGT REV: ACACTCTTTCCCTACACGACGCTCTTCCGATCTGTAGCTCTTGTCTGGAGAT CC

5425C>T FW: GTGACTGGAGTTCAGACGTGTGCTCTTCCGATCTGAAGCCATTGTCCAGTCTATC

5425C>T REV: ACACTCTTTCCCTACACGACGCTCTTCCGATCTGGTACAAGTTAAGGCACACAG

6513T>A FW: GTGACTGGAGTTCAGACGTGTGCTCTTCCGATCTGACTCAGTCTGACAGAGTTCTC

6513T>A REV: ACACTCTTTCCCTACACGACGCTCTTCCGATCTCTAGTTCTGTCCACTGGTCC

6619C>T FW: GTGACTGGAGTTCAGACGTGTGCTCTTCCGATCTTGCCTTCCGTTCCAGTTACC

6619C>T REV: ACACTCTTTCCCTACACGACGCTCTTCCGATCTGAGCTCTTGGTTGCAGGGAT

The primers used for the second amplification PCR reaction which include the unique indexes employed to identify different sequencing products were the following:

Primer 1.0 FW: AATGATACGGCGACCACCGAGATCTACACACACTCTTTCCCTACACGACGCTCTTC CGATCT

Primer 1.0 SIC2 FW: AATGATACGGCGACCACCGAGATCTACACAATGAAACACTCTTTCCCTACA CGACGCTCTTCCGATCT

Common REV: GTGACTGGAGTTCAGACGTGTGCTCTTCCGATCT

Index 1 REV: CAAGCAGAAGACGGCATACGAGATAAATAGATGGTGACTGGAGTTC

Index 2 REV: CAAGCAGAAGACGGCATACGAGATCAGAGGAGAGTGACTGGAGTTC

Index 3 REV: CAAGCAGAAGACGGCATACGAGATCGTATAGATGTGACTGGAGTTC

Index 4 REV: CAAGCAGAAGACGGCATACGAGATAAGGGCTCAGTGACTGGAGTTC